A CMOS Inductorless MedRadio OOK Transceiver With a 42 μW Event-Driven Supply-Modulated RX and a 14% Efficiency TX for Medical Implants

Mao-Cheng Lee[1], Alireza Karimi-Bidhendi[1], Omid Malekzadeh-Arasteh[1],
Po T. Wang[2], Zoran Nenadic[2], An H. Do[3], and Payam Heydari[1],
[1]Department of Electrical Engineering and Computer Science, University of California, Irvine, CA, 92697, USA
[2]Department of Biomedical Engineering, University of California, Irvine, CA, 92697, USA
[3]Department of Neurology, University of California, Irvine, CA, 92697, USA

***Abstract*—An inductorless MedRadio (413∼419 MHz) OOK transceiver for an implantable brain-machine interface (BMI) in 180 nm CMOS is presented. An event-driven supply modulation (EDSM) technique is introduced in the receiver to lower the power consumption to 42/92 μW at 1/10 kbps, achieving −79/−74 dBm sensitivity (at 0.1% BER). The transmitter employs a current-starved ring oscillator with an automatic frequency calibration loop, achieving 14% efficiency for random OOK data at −4 dBm output power. Wireless connection, benchtop, multi-user coexistence, and *in-vitro* phantom test results are demonstrated.**

***Index Terms*—Transceiver, inductorless, MedRadio band, implantable, brain-machine interface, event-driven, supply modulation.**

I. Introduction

A growing interest in fully implantable medical devices (IMDs) for emerging applications, such as BMIs or artificial organs, necessitates the development of low-power wireless transceivers (TRXs) to transfer data. Fig. 1 shows an example of one such implantable BMI system that could potentially restore the ability to walk in those with spinal cord injury. This system can be envisioned to encompass a skull unit that can sense μV-level brain signals. The signals would be routed out of the skull unit by a tunneling cable (similar to modern deep-brain stimulators [1]), and delivered to a chest-wall unit (CWU). The CWU would process brain signals to detect walking intentions and convert them into low data-rate (1∼10 kbps) wireless commands for external prostheses, such as exoskeletons.

Stringent performance requirements and power constraints of fully implantable BMIs require system architectures capable of executing multiple functions (e.g., sensing, stimulation and communication), while achieving a small surgical footprint, reduced heat dissipation and prolonged battery life. It can be estimated that a wireless TRX would consume a large portion of BMI power, thereby creating a major bottleneck for system design. Existing MedRadio low-power TRX architectures [2]–[5] employ bulky on- or off-chip inductors for impedance matching and/or performance improvements. In contrast, this work presents a CMOS low-power inductorless OOK TRX,

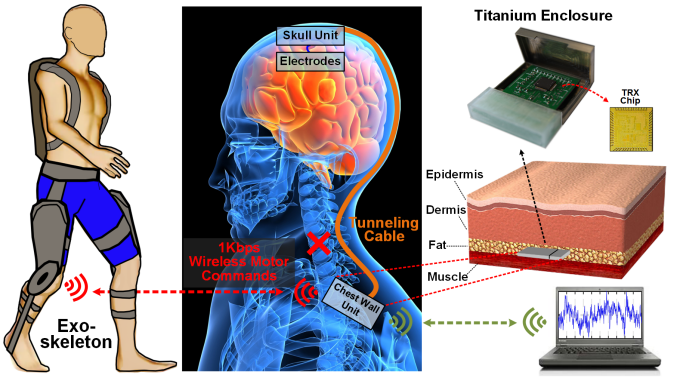

Fig. 1. Proposed fully-implantable BMI system for restoration of walking, with a signal acquisition front-end (skull unit) and signal processing and wireless communication modules (chest wall unit). This system bypasses the injured spinal cord and enables direct brain control of an exoskeleton.

operating in MedRadio 413∼419 MHz band, to transfer BMI control commands. To achieve low-power operation, an event-driven supply modulation (EDSM) technique on the RX side and fast start-up power-cycling on the TX side are introduced. The rest of this paper is organized as follows: Section II presents the TRX circuit implementation. Measurement results are shown in Section III and a conclusion in Section IV.

II. Circuit Implementation

Fig. 2 shows the proposed TRX architecture. The time-division-duplex TRX is designed to communicate with exoskeletons and external MedRadio station at 1∼10 kbps data-rate. It consists of an EDSM RX, a direct-modulation TX, a SPI interface and an on-chip T/R switch.

A. Event-Driven Supply Modulation Receiver

The system architecture and schematic of the EDSM RX are shown in Fig. 3. The noise-cancelling LNA (common-gate/common-source differential stage [6] followed by capacitively-degenerated gain stages and a differential-to-single-ended buffer) provides 50 Ω matching to the antenna. In order to match the noise-cancelling LNAs input to the antenna, a large current (1.5∼ 2mA) is needed. A power-saving mechanism is thus introduced, which constitutes an

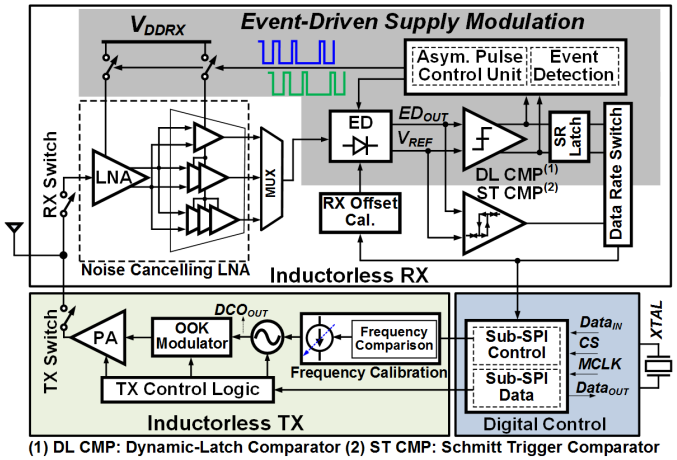

Fig. 2. The architecture of the proposed low-power OOK TRX.

event detection circuitry and a delay control unit to generate and adjust narrow asymmetric pulses. The system clock (CLK_{SYS}) running at Nyquist rate of the baseband (BB) signal periodically activates the LNA to strobe the received signal for subsequent non-coherent detection. The common-source-based envelope detector employs a class-AB biasing structure to maximize responsivity, thus relaxing the input-referred offset and sensitivity constraints of the following latch-based dynamic comparator. As shown in Fig. 4, completion of the comparators decision after a regenerative time (T_{CMP}), which is dependent on the comparator input signal, marks an event at which the output is captured in an SR latch and fed to the event detection circuitry. The event detection logic is triggered by the comparator differential output and CLK_{SYS}, generating the falling edges of narrow pulses, $SM_{\phi 1}$, to turn off the power-hungry LNA and amplifiers until the next strobing edge. Since the LNA and amplifiers dominates the total power consumption by >99%, the average power consumption of RX with EDSM technique can be approximated as:

$$P_{average} \cong P_{total} \times \left(\frac{T_{on}}{T_{clk,sys}}\right) \quad (1)$$

where P_{total} is the total power consumption of RX without EDSM technique, T_{on} is the on-period of power-hungry blocks and $T_{clk,sys}$ refers to sampling period of the system clock. The advantage of EDSM technique can be leveraged by making $T_{on} \ll T_{clk,sys}$ in the expression such that the average power consumption is significantly reduced.

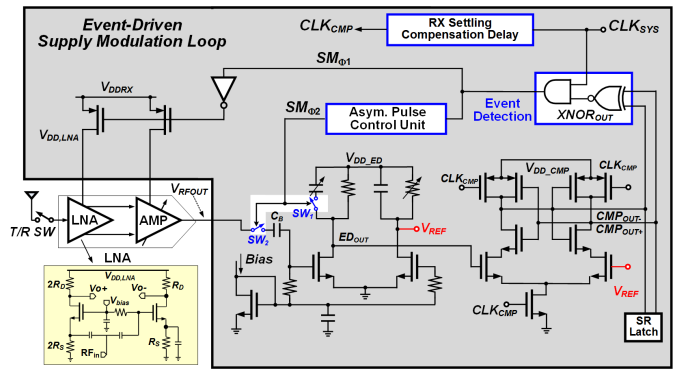

Fig. 3. Event-driven supply modulation RX schematic.

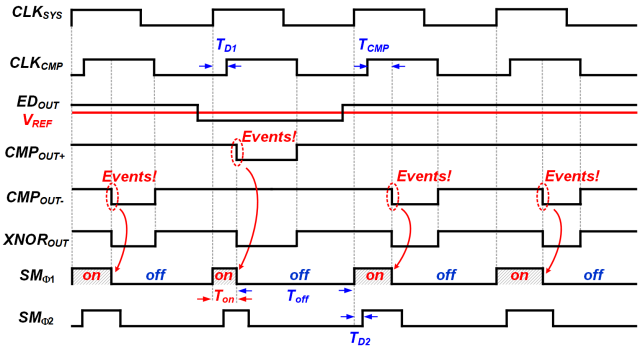

Fig. 4. The timing diagram of EDSMRX.

To realize infinitesimal values for T_{on}, one requires very narrow pulses, however, proper functionality of the circuit may not be guaranteed under such short periods of time. The minimum value of T_{on} is dictated by the settling time and propagation delay of individual blocks. Thus, proper timing of $SM_{\phi 1}$ and $SM_{\phi 2}$ is required to minimize the amplifier-slewing and settling time of RX. First, to conserve the charge on the bypass capacitor (C_B) between on/off phases, an asynchronous pulse control unit applies a T_{D2}-delayed version of $SM_{\phi 1}$ to two switches (SW_1 and SW_2) which prevents amplifier-slewing and reduces the envelope detector settling time. Secondly, the RX settling compensation unit delays CLK_{SYS} by T_{D1} to allow the RX to reach its bias operating point. The proposed EDSM technique thereby reduces the RX power consumption by 99.6% to 42 μW at 1 kbps and by 99.1% to 92 μW at 10 kbps.

B. Direct-Modulation Transmitter

Depicted in Fig. 5 is the TX architecture, comprising a free-running digitally-controlled ring oscillator (DCO) with automatic frequency calibration (AFC), OOK-modulating T-switch, and a self-biased amplifier driving an inverter-based PA. Availability of the 6 MHz continuous MedRadio band allows for low-power DCO with relaxed phase-noise requirement, particularly for constant-amplitude modulation schemes. The oscillator's frequency (f_{osc}) is controlled by 5-bit coarse- and 5-bit fine-tuned current mirrors from SPI and AFC, respectively, to compensate for PVT variations. Additionally, the DCO offers a fast turn-on time and requires no start-up circuitry, allowing the TX to be power-cycled by the baseband data for data rates as high as 0.4 Mbps. Due to power-

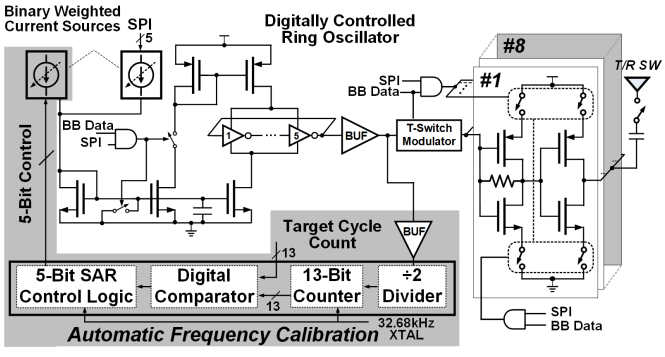

Fig. 5. Direct-modulation transmitter and automatic frequency calibration.

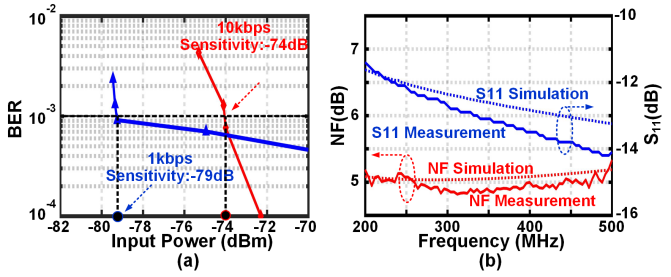

Fig. 6. EDSM Receiver measured BER with different data-rate (a) and the measured S11 and NF (b).

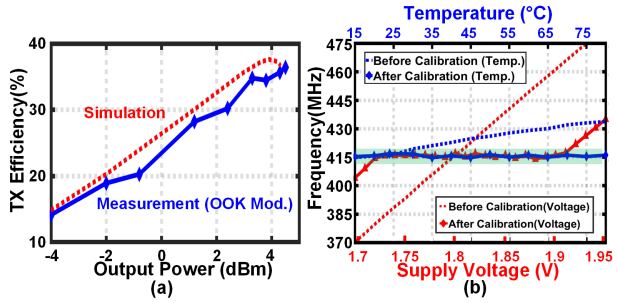

Fig. 7. Transmitter output power vs. efficiency (a) and the frequency variation with an without AFC (b).

cycling, the TX does not have undesired power emission when transmitting 0s. The PA output power can be configured using PA switches. Within AFC block, the 13-bit counter computes the binary representation of $f_{osc}/2$ cycles over the 32.768 kHz reference clock period provided by a 36 μW on-chip crystal oscillator. The result is compared with the target cycle count N_{CYC}, where $N_{CYC} = f_{osc}/(2f_{XTAL})$, and fed to a SAR logic to adjust the oscillator current, thereby fine-tuning f_{osc} across 80 MHz frequency range within an estimated 0.47 ms calibration time.

III. Measurement Results

A. Electrical Measurements

Fig. 6 (a) displays the RX measured BER under different data-rate conditions. The measured BER curves for 1 and 10 kbps yield a sensitivity of -79 and -74 dBm at 0.1% BER with PN15 data sequence. The measured (and simulated) RX S_{11} and noise figure are -13.5 (-13) dB and -4.9 (-5) dB at 416 MHz respectively, as shown in Fig. 6 (b). Fig. 7 (a) shows the measured and simulated TX efficiency versus output power. The TX output power varies from -4 to 4.5 dBm, yielding efficiency of 14% to 36% for OOK modulation

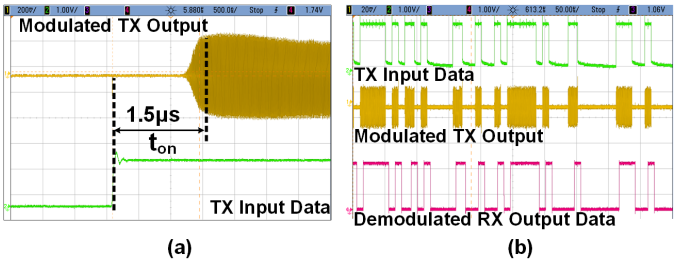

Fig. 8. (a) Transmitter start-up time (b) functional wireless data transmission measurement.

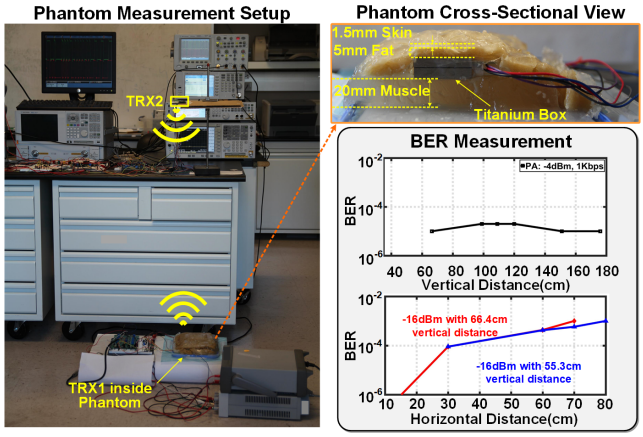

Fig. 9. *in-vitro* phantom measurement setup and measured BER results.

and 7% to 18% in continuous-wave (CW) mode, respectively. AFC periodically monitors the TX carrier frequency, f_c, and is designed to improve frequency-drift tolerance from 19% to 0.24% across 1.73∼1.9V supply interval and from 4.6% to 0.3% across 15∼78°C temperature range (Fig. 7 (b)). Fig. 8 (a) and (b) show the measured TX start-up time (1.5 μs) and wireless transmission of a random data, respectively.

B. In-Vitro Phantom Measurements

Fig. 9 presents the *in-vitro* phantom test and wireless connection setup. To account for signal attenuation through the body tissue, a human-like phantom was assembled to mimic the electrical properties. This phantom is composed of 3 layers, emulating the conductivity, permittivity and thickness of the human skin, fat, and muscle in chest area [7], [8]. The measured conductivity of skin, fat and muscle layers is 0.77, 0.034, 0.8 S/m respectively. The measured permittivity is 49.1, 5.54 and 57.4 accordingly. To further assess feasibility in real-world scenarios where BMI and end effectors' positions may vary, the relative position of TRXs were modified based on plausible distances. The BER remains $< 0.1\%$ for a maximum vertical distance of 1.8 m. Similarly, the BER remains $< 0.1\%$ for a maximum horizontal distance of 0.8 m while the position of TRX2 is fixed.

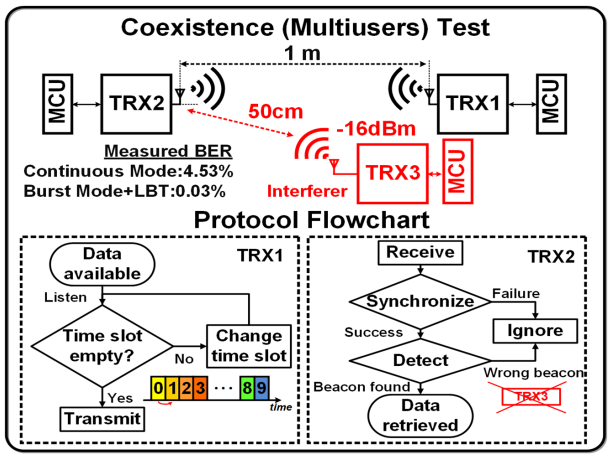

Fig. 10. The coexistence test setup and the flowchart of listen-before-talk protocol.

TABLE I
RECEIVER PERFORMANCE COMPARISON

Reference	ISSCC 2014 [2]	TMTT 2014 [3]	TCAS-I 2016 [4]	JSSC 2016 [9]	JSSC 2016 [10]	This Work
Process (nm)	40	180	180	65	65	180
Carrier Frequency (MHz)	402∼405 / 420∼450	403/433	402∼405	2400	915	413∼419
Supply Voltage (V)	1	1.2	0.45	0.5	1	1.5
Architecture	Zero-IF	Direct Conv.	Low-IF	Dual-IF	TX-referenced	Non-coherent EDSM
Modulation	GMSK/DBPSK	ASK	OOK/FSK	OOK	BPSK	OOK
Inductor Type	Off-Chip	Off-Chip	On-Chip	Off-Chip	Off-Chip	None
Data Rate (kbps)	11.7/562/4500	10	50/120	10	10	1/10
Sensitivity (dBm)	-112/-93/-83	-72/-73	-55/-53.5	-97	-76	-79/-74
Power	2.19 mW	2.19 mW	352 μW	99 μW	135 μW	42 μW/92 μW

TABLE II
TRANSMITTER PERFORMANCE COMPARISON

Reference	ISSCC 2014 [2]	TMTT 2014 [3]	JSSC 2009 [5]	This Work
Process (nm)	40	180	180	180
Carrier Freq. (MHz)	402∼405 420∼450	403	403	413∼419
Supply (V)	1	1.2	1.8	1.8
Architecture	Polar/Direct Mod.	Direct Mod.	Direct Mod.	Direct Mod.
Modulation	GMSK / DBPSK	OOK / OQPSK	FSK	OOK
Inductor Type	Off-Chip	Off-Chip	On-Chip	None
Output Power (dBm)	-10/-17	-20.9/-17	-20∼0	-4∼4.5
Data Rate (kbps)	11/4500	100/1000	50	1/10
Efficiency	NA	NA	33%[a] @-5 dBm	14%(OOK) 7%(CW)
Power (mW)	2.27/2.28	3.32	4.9	2.8[b] 5.6[c]

[a]PA only. [b]With -4 dBm output power in OOK mode. [c]With -4 dBm output power in CW mode.

C. Multi Users Coexistence Testing

A practical issue of BMI is the potential interference between multiple users operating in the vicinity of one another. A listen-before-talk protocol with the TRX operating in burst-mode data transfer operation was implemented (*cf.* Fig. 10) to address coexistence with an interferer, TRX3, by advancing through 10 time slots to find an available one for exclusive pairing. An exemplary coexistence scenario is demonstrated, where the distance between TRX3 and TRX2 is shorter than that between TRX1 and TRX2 by 0.5 m. This protocol improves BER from 4.53% (continuous mode) to 0.03%.

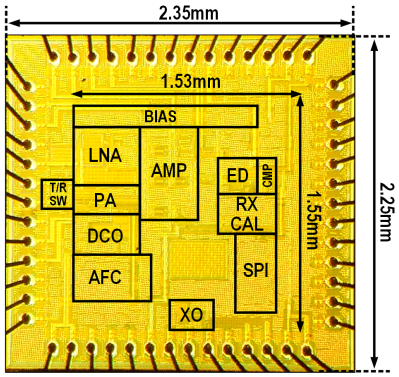

Fig. 11. Chip micrograph with main circuit blocks labeled.

IV. CONCLUSION

Table I and Table II summarize the performance of proposed TRX and the comparison with prior art. The 180 nm CMOS inductorless TRX occupies 2.35 $\times$ 2.25 mm^2 of die area including pads (Fig. 11), and requires no off-chip components except an antenna. The proposed non-coherent EDSM RX achieves $-79/-74$ dBm sensitivity and dissipates 42/92 μW at 1/10 kbps, respectively.

ACKNOWLEDGMENT

This research is funded by the National Science Foundation, award #1446908. The authors thank TowerJazz Semiconductor for chip fabrication and D. Huh from Keysight Technologies for providing measurement equipment.

REFERENCES

[1] *DBS^{TM} Extension Kit for Deep Brain Stimulation*, Medtronic.
[2] M. Vidojkovic, X. Huang, X. Wang, C. Zhou, A. Ba, M. Lont, Y. H. Liu, P. Harpe, M. Ding, B. Busze, N. Kiyani, K. Kanda, S. Masui, K. Philips, and H. de Groot, "9.7 A 0.33nJ/b IEEE802.15.6/proprietary-mics/ism-band transceiver with scalable data-rate from 11kb/s to 4.5mb/s for medical applications," in *2014 IEEE International Solid-State Circuits Conference Digest of Technical Papers (ISSCC)*, 2014, pp. 170–171.
[3] H. C. Chen, M. Y. Yen, Q. X. Wu, K. J. Chang, and L. M. Wang, "Batteryless transceiver prototype for medical implant in 0.18-mum cmos technology," *IEEE Trans. Microwave Theory Tech.*, vol. 62, no. 1, pp. 137–147, Jan 2014.
[4] J. Y. Hsieh, Y. C. Huang, P. H. Kuo, T. Wang, and S. S. Lu, "A 0.45-v low-power ook/fsk rf receiver in 0.18 μm cmos technology for implantable medical applications," *IEEE Trans. Circuits Syst. I Regul. Pap.*, vol. 63, no. 8, pp. 1123–1130, 2016.
[5] N. Cho, J. Bae, and H. J. Yoo, "A 10.8 mw body channel communication/mics dual-band transceiver for a unified body sensor network controller," *IEEE J. Solid-State Circuits*, vol. 44, no. 12, pp. 3459–3468, 2009.
[6] F. Bruccoleri, E. A. M. Klumperink, and B. Nauta, "Wide-band cmos low-noise amplifier exploiting thermal noise canceling," *IEEE J. Solid-State Circuits*, vol. 39, no. 2, pp. 275–282, 2004.
[7] T. Karacolak, A. Z. Hood, and E. Topsakal, "Design of a dual-band implantable antenna and development of skin mimicking gels for continuous glucose monitoring," *IEEE Trans. Microwave Theory Tech.*, vol. 56, no. 4, pp. 1001–1008, 2008.
[8] A. T. Mobashsher and A. M. Abbosh, "Artificial human phantoms: Human proxy in testing microwave apparatuses that have electromagnetic interaction with the human body," *IEEE Microwave Mag.*, vol. 16, no. 6, pp. 42–62, 2015.
[9] C. Salazar, A. Cathelin, A. Kaiser, and J. Rabaey, "A 2.4 ghz interferer-resilient wake-up receiver using a dual-if multi-stage n-path architecture," *IEEE J. Solid-State Circuits*, vol. 51, no. 9, pp. 2091–2105, 2016.
[10] D. Ye, R. van der Zee, and B. Nauta, "A 915 mhz 175 μW receiver using transmitted-reference and shifted limiters for 50 db in-band interference tolerance," *IEEE J. Solid-State Circuits*, vol. 51, no. 12, pp. 3114–3124, 2016.